Dyes and Pigments 95 (2012) 161–167

Contents lists available at SciVerse ScienceDirect

Dyes and Pigments

journal homepage: www.elsevier.com/locate/dyepig

Room-temperature phosphorescence in solution and in solid state from purely organic dyes

Guoping Yong*, Wenlong She, Yiman Zhang

Department of Chemistry, University of Science and Technology of China, Hefei 230026, PR China

ARTICLE INFO

Article history:
Received 20 December 2011
Received in revised form
6 March 2012
Accepted 5 April 2012
Available online 17 April 2012

Keywords:
(*E*)-3-benzylideneimidazo[1,2-*a*]pyridin-2(3*H*)-one derivatives
Phosphorescent dyes
One-pot synthesis
Phosphorescent colors
Solid state
Room-temperature phosphorescence

ABSTRACT

Phosphorescence has seldom been observed in purely organic dyes in the solution at room temperature. We herein report efficient phosphorescence in the solution from (*E*)-3-benzylideneimidazo[1,2-*a*]pyridin-2(3*H*)-one and its derivatives. This opens up a new class of purely organic dyes to applications in the phosphor design. In the solid state, the ordered columnar stacking arrangements, intermolecular close contacts, and lateral intermolecular hydrogen bonding interactions between neighboring columns make these luminogenic molecules highly phosphorescent at room temperature, and lead to phosphorescent color changes (from yellow in the solution to aurantiacus–red in the solid state). Here, using these luminogenic molecules, a series of new purely organic phosphors are color-tuned to emit yellow, aurantiacus, orange, nacarat and red in the solid state, which are promising candidates for potential applications in organic light-emitting diodes for display.

1. Introduction

Organic conjugated compounds are nowadays still the focus of intense investigations in the field of organic electronics, due to their appealing applications such as electroluminescent devices, sensors, lasers, and other semiconductor devices. The development of efficient solid luminescent materials, however, is still a challenging issue, because many dyes are highly emissive in dilute solutions but become weakly luminescent or even nonemissive in the condensed phase, attributed to the formation of detrimental excimers and exciplexes in the condensed phase [1]. Such an aggregation-caused quenching (ACQ) problem must be overcome, because luminogenic molecules are commonly used as the condensed states. Although various chemical, physical, and engineering approaches have been used to solve the ACQ effect [2], the attempts have met with only limited success. Fortunately, some purely organic molecules that can display efficient aggregation-induced emissions in the solid states have been reported [3].

To date, purely organic luminogenic molecules that are also phosphorescent are very rare [4], in contrast to metal-containing materials, because the highly bonded nature of electrons in metal-free organic molecules makes them little free and less impetus to emit from triplet states. Phosphorescence is therefore generally regarded as a solely inorganic or organometallic property. The phosphorescent emission of purely organic materials is so weak and ineffective that they fail to enter discussions on modern phosphorescent applications [5]. However, the development of phosphorescent dyes is a goal of intensive research because of their high application potentials in organic electronics, as well as chemical and biological detection [6]. Although most purely organic materials have been widely considered to be non-phosphorescent in character, very recently, crystallization-induced phosphorescence of the purely organic materials has been reported [7], probably attributable to aromatic carbonyls, the heavy halogen atom effect, or halogen bonding.

On the basis of 2,3′-biimidazo[1,2-*a*]pyridin-2′-one ($Hbipo^{-\bullet}$) radical and its derivatives, our group recently reported a series of purely organic luminescent materials which also display unique magnetic properties [8], and coordination polymers which exhibit interesting magnetic properties and various luminescent colors, including direct white-light phosphorescent emission [9]. Very recently, we discovered two purely organic solid phosphorescent materials based on 2-(imidazo[1,2-*a*]pyridin-2-yl)-2-oxoacetic acid radical, which exhibit excitation wavelength independent of direct white-light and blue-light

* Corresponding author. Tel.: +86 551 360 1584; fax: +86 551 360 1592.
E-mail address: gpyong@ustc.edu.cn (G. Yong).

0143-7208/$ – see front matter © 2012 Elsevier Ltd. All rights reserved.
doi:10.1016/j.dyepig.2012.04.003

phosphorescent emission, respectively [10]. The phosphorescence can derive from carbonyl group which exhibit somewhat spin–orbit coupling at the carbonyl oxygen that allows for intrinsic triplet generation through intersystem crossing [7b,11].

In an effort to explore the novel purely organic phosphorescent materials based on imidazo[1,2-*a*]pyridin-2-ones, we designed and synthesized a new class of organic conjugated compounds ((*E*)-3-benzylideneimidazo[1,2-*a*]pyridin-2(3*H*)-one derivatives, Fig. 1) to examine their room-temperature phosphorescent characters in the solution and solid state. To the best of our knowledge, this is the first report on the evaluation of the phosphorescent properties in the solution and solid state of (*E*)-3-benzylideneimidazo[1,2-*a*]pyridin-2(3*H*)-one derivatives. We are aware of only two works reporting the synthesis of few (*E*)-3-benzylidene- imidazo[1,2-*a*]pyridin-2(3*H*)-ones [12] and no photophysical characterization for these compounds was given.

2. Experimental

2.1. Materials and methods

All reagents were of analytical grades, and obtained from commercial vendors and used without further purification. ^{1}H and ^{13}C NMR spectra were obtained on Bruker Avance 400 MHz NMR spectrometers using DMSO-d_6 as solvent and tetramethylsilane (TMS) as the internal standard. High-resolution mass spectra (HRMS) were obtained on Micromass GCT-MS instrument operating in electron impact (EI) mode and time of flight (TOF) mass detector. UV/vis absorption spectra were measured using UV-3100 spectrophotometer in DMF and DMSO solutions at 298 K. The solution (10 μM DMF) and solid photoluminescence (PL) spectra, and the decay lifetimes were determined at room temperature on a Fluorolog-3-TAU fluorescence spectrophotometer. The CIE-1931 chromaticity coordinates were calculated using a Color-Coordinate.exe program. The same results can also be obtained using a gocie.exe program from http://www.geocities.com/krjustin/gocie.html. The quantum yields of solution state were measured at room temperature in a 10 μM DMF solution using quinine sulfate ($\Phi = 0.54$) as a reference. Corrections were made due to the change in solvent refractive indices [13]. The quantum yields of solid state were measured on a Fluorolog-3-TAU fluorescence spectrophotometer equipped with a $BaSO_4$-coated integrating sphere, upon excitation at 365 nm.

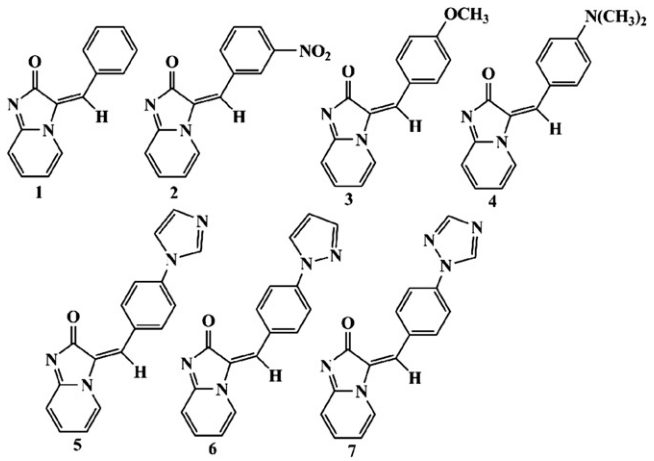

Fig. 1. (*E*)-3-benzylideneimidazo[1,2-*a*]pyridin-2(3*H*)-one derivatives.

2.2. Synthesis

2.2.1. (*E*)-3-benzylideneimidazo[1,2-a]pyridin-2(3H)-one (**1**)

A mixture of hydrochloride salt of imidazo[1,2-*a*]pyridin-2(3*H*)-one (1.72 g, 10 mmol) and benzaldehyde (1.06 g, 10 mmol) in acetic acid (50 mL) was heated at 125 °C for 2.5 h. After cooled to room temperature, the resulting orange solid was collected by filtration and washed with ethanol. The orange solid was immersed in saturated $NaHCO_3$ solution until no bubble was observed. The solid then was filtered out and washed with water and ethanol; recrystallization of orange solid from DMF solution afforded orange crystals which are suitable for X-ray single-crystal diffraction analysis. Yield: 1.59 g (7.16 mmol), 71.6%. ^{1}H NMR (400 MHz, DMSO-d_6, 25 °C, ppm): 8.67 (d, $J = 6.8$ Hz, 1H), 8.48 (dd, $J = 6.6$ Hz, 3.0 Hz, 2H), 7.94 (s, 1H), 7.74 (ddd, $J = 8.6$ Hz, 7.0 Hz, 1.3 Hz, 1H), 7.51 (dd, $J = 5.1$ Hz, 1.9 Hz, 3H), 7.06 (d, $J = 8.9$ Hz, 1H), 6.86 (td, $J = 6.9$ Hz, 1.1 Hz, 1H). ^{13}C NMR (101 MHz, DMSO-d_6, 25 °C, ppm): 172.82, 162.72, 141.56, 132.02, 131.87, 131.32, 129.80, 128.32, 127.86, 114.69, 111.34. HRMS (EI, *m*/*z*, $[M]^+$): Calc. for $C_{14}H_{10}N_2O$: 222.24, Found: 222.22.

2.2.2. Compounds **2**–**7**

Under the same reaction conditions as **1**, the reactions by the replacement of benzaldehyde with different benzaldehyde derivatives afforded a series of (*E*)-3-benzylideneimidazo[1,2-*a*]pyridin-2(3*H*)-one derivatives.

*2.2.2.1. (E)-3-(3′-nitrobenzylidene)imidazo[1,2-a]pyridin-2(3H)-one (**2**).* Nacarat crystals, yield: 2.05 g (7.68 mmol), 76.8%. ^{1}H NMR (400 MHz, DMSO-d_6, 25 °C, ppm): 9.48 (s, 1H), 8.76 (d, $J = 7.8$ Hz, 1H), 8.63 (d, $J = 6.8$ Hz, 1H), 8.34 (d, $J = 7.8$ Hz, 1H), 8.09 (s, 1H), 7.84–7.75 (m, 2H), 7.09 (d, $J = 8.8$ Hz, 1H), 6.89 (t, $J = 6.8$ Hz, 1H). ^{13}C NMR (101 MHz, DMSO-d_6, 25 °C, ppm): 172.85, 163.53, 149.39, 147.70, 142.44, 137.82, 133.32, 131.20, 129.99, 129.90, 125.96, 125.30, 125.14, 114.96, 111.72. HRMS (EI, *m*/*z*, $[M]^+$): Calc. for $C_{14}H_9N_3O_3$: 267.24, Found: 267.21.

*2.2.2.2. (E)-3-(4′-methoxybenzylidene)imidazo[1,2-a]pyridin-2(3H)-one (**3**).* Aurantiacus crystals, yield: 1.91 g (7.58 mmol), 75.8%. ^{1}H NMR (400 MHz, DMSO-d_6, 25 °C, ppm): 8.69–8.53 (m, 3H), 7.89 (s, 1H), 7.74–7.64 (m, 1H), 7.11–6.99 (m, 3H), 6.83 (td, $J = 6.9$ Hz, 1.1 Hz, 1H), 3.86 (s, 3H). ^{13}C NMR (101 MHz, DMSO-d_6, 25 °C, ppm): 173.04, 162.00, 161.81, 140.62, 134.64, 129.38, 128.00, 127.40, 124.83, 114.52, 113.96, 111.15, 55.45. HRMS (EI, *m*/*z*, $[M]^+$): Calc. for $C_{15}H_{12}N_2O_2$: 252.27, Found: 252.28.

*2.2.2.3. (E)-3-(4′-(dimethylamino)benzylidene)imidazo[1,2-a]pyridin-2(3H)-one (**4**).* Bright orange red crystals, yield: 2.12 g (8.0 mmol), 80%. ^{1}H NMR (400 MHz, DMSO-d_6, 25 °C, ppm): 8.62 (d, $J = 6.8$ Hz, 1H), 8.60–8.52 (m, 2H), 7.79 (s, 1H), 7.65–7.58 (m, 1H), 7.02 (d, $J = 8.9$ Hz, 1H), 6.84–6.75 (m, 3H), 3.07 (s, 6H). ^{13}C NMR (101 MHz, DMSO-d_6, 25 °C, ppm): 173.10, 160.10, 152.49, 138.87, 135.00, 129.13, 128.68, 124.47, 119.79, 114.15, 111.15, 110.76, 40.31, 40.20. HRMS (EI, *m*/*z*, $[M]^+$): Calc. for $C_{16}H_{15}N_3O$: 265.31, Found: 265.31.

*2.2.2.4. (E)-3-(4′-(1H-imidazol-1-yl)benzylidene)imidazo[1,2-a]pyridin-2(3H)-one (**5**).* Orange red crystals, yield: 1.26 g (4.34 mmol), 43.4%. ^{1}H NMR (400 MHz, DMSO-d_6, 25 °C, ppm): 8.65 (t, $J = 8.0$ Hz, 3H), 8.43 (s, 1H), 7.96 (s, 1H), 7.89 (t, $J = 1.3$ Hz, 1H), 7.86–7.82 (m, 2H), 7.77–7.69 (m, 1H), 7.16 (s, 1H), 7.07 (d, $J = 8.9$ Hz, 1H), 6.86 (td, $J = 6.9$ Hz, 1.1 Hz, 1H). ^{13}C NMR (101 MHz, DMSO-d_6, 25 °C, ppm): 172.96, 162.71, 141.55, 138.52, 135.58, 133.82, 130.29, 130.22, 129.70, 129.46, 126.68, 119.42, 117.62, 114.75, 111.41. HRMS (EI, *m*/*z*, $[M]^+$): Calc. for $C_{17}H_{12}N_4O$: 288.30, Found: 288.32.

*2.2.2.5. (E)-3-(4′-(1H-pyrazol-1-yl)benzylidene)imidazo[1,2-a]pyridin-2(3H)-one (**6**).* Aurantiacus crystals, yield: 1.65 g (5.73 mmol), 57.3%. ^{1}H NMR (400 MHz, DMSO-d_6, 25 °C, ppm): 8.66 (dd, J = 11.0 Hz, 5.7 Hz, 4H), 8.05–7.94 (m, 3H), 7.83 (d, J = 1.5 Hz, 1H), 7.73 (ddd, J = 8.4 Hz, 7.0 Hz, 1.2 Hz, 1H), 7.07 (d, J = 8.9 Hz, 1H), 6.86 (td, J = 6.9 Hz, 1.0 Hz, 1H), 6.65–6.57 (m, 1H). ^{13}C NMR (101 MHz, DMSO-d_6, 25 °C, ppm): 172.95, 162.54, 141.82, 141.40, 141.23, 133.73, 129.68, 129.66, 129.17, 128.08, 126.98, 117.68, 114.71, 111.38, 108.58. HRMS (EI, m/z, [M]$^+$): Calc. for $C_{17}H_{12}N_4O$: 288.30, Found: 288.29.

*2.2.2.6. (E)-3-(4′-(1H-1,2,4-triazol-1-yl)benzylidene)imidazo[1,2-a]pyridin-2(3H)-one (**7**).* Orange red crystals, yield: 1.86 g (6.43 mmol), 64.3%. ^{1}H NMR (400 MHz, DMSO-d_6, 25 °C, ppm): 9.43 (s, 1H), 8.71–8.63 (m, 3H), 8.30 (s, 1H), 8.05–7.98 (m, 3H), 7.78–7.71 (m, 1H), 7.07 (d, J = 8.9 Hz, 1H), 6.87 (td, J = 6.9 Hz, 1.1 Hz, 1H). ^{13}C NMR (101 MHz, DMSO-d_6, 25 °C, ppm): 172.74, 162.78, 154.11, 142.75, 139.40, 133.62, 131.48, 129.57, 128.65, 126.06, 121.79, 118.80, 114.79, 111.46. HRMS (EI, m/z, [M]$^+$): Calc. for $C_{16}H_{11}N_5O$: 289.29, Found: 289.28.

2.3. Single-crystal X-ray crystallography

The X-ray diffraction measurement for **1** was performed on a Gemini S Ultra CCD diffractometer (Oxford diffraction Ltd.) using graphite monochromated Cu-Kα radiation (λ = 1.54184 Å). The structure was solved by direct method and refined with full-matrix least-squares technique on F^2 by using the SHELXS-97 and SHELXL-97 programs [14]. The empirical absorption correction (SCALE3 ABSPACK) was applied. All non-hydrogen atoms were refined with anisotropic displacement parameters. The hydrogen atoms were placed in geometrically calculated positions. Weighted R factor (R_w) and all goodness of fit S are based on F^2, conventional R factor (R) is based on F.

3. Results and discussion

3.1. Syntheses and crystal structure description

As described in Scheme 1, the reaction between hydrochloride salt of imidazo[1,2-*a*]pyridin-2(3*H*)-one and benzaldehyde derivatives afforded a series of (*E*)-3-benzylideneimidazo[1,2-*a*]pyridin-2(3*H*)-one derivatives by one-pot synthesis method, and the orange single crystals, (*E*)-3-benzylideneimidazo[1,2-*a*] pyridin-2(3*H*)-one (**1**) were obtained. Compound **1** crystallizes in triclinic space group *P*-1. The molecular structure of **1** is shown in Fig. 2. Interestingly, compound **1** exhibits the trans-configuration. According to the mechanism of the Pschorr cyclization, the condensation of imidazo [1,2-*a*]pyridin-2(3*H*)-one with benzaldehyde should have the cis-configuration of the phenyl and pyridyl groups, however, the product was the trans-compound. Abramovitch and Hey have reported that (*E*)-3-(2′-nitrobenzylidene)imidazo[1,2-*a*]pyridin-2(3*H*)-one was the trans-configuration [12b]. They think that it seems likely that there is dipolar repulsion between the pyridine nitrogen atom and the electronegative nitro group, leading to the observed stereochemistry.

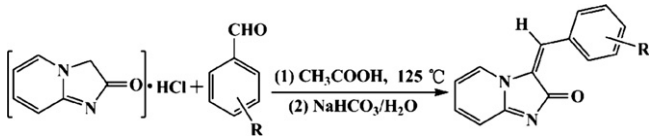

Scheme 1. Synthesis of (*E*)-3-benzylideneimidazo[1,2-*a*]pyridin-2(3*H*)-one derivatives.

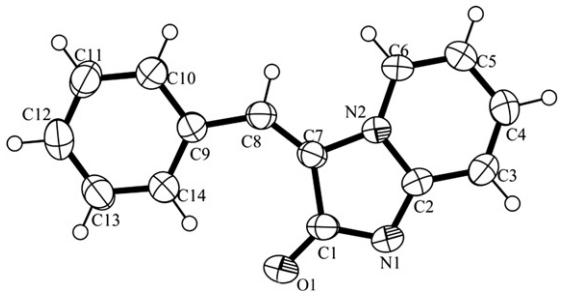

Fig. 2. ORTEP diagram of molecular structure of **1** with ellipsoids drawn at 50% probability.

Compound **1** forms one-dimensional (1D) columnar stacking chain along the *b*-axis, in which the molecules appear to be a slightly slipped stack. In 1D chain, (*E*)-3-benzylideneimidazo[1,2-*a*]pyridin-2(3*H*)-one molecules adopt slipped head-to-tail stacking modes, as shown in Fig. 3. Although the stacking distance is outside van der Waals contact, there exist four kinds of intermolecular close contacts (C1···C7′ of 3.336 Å, C6···C10′ of 3.369 Å, C7···C9′ of 3.391 Å, and C8···C8′ of 3.257 Å, shorter than van der Waals) between neighboring molecules. The columnar chains are further assembled into two-dimensional (2D) supramolecular network via lateral intermolecular C14–H···N1′ hydrogen bonds (3.155 Å) between neighboring columns, as shown in Fig. S1 (in the Supporting information).

3.2. UV/vis absorption spectra of compounds **1**–**7**

The UV/vis absorption spectra of all seven compounds were measured at room temperature in DMF solution (Fig. 4). Even if measured in DMSO solution (Fig. S2, in the Supporting Information), these compounds exhibit similar UV/vis absorption spectra in DMF solution. Except for compound **4**, other six compounds display intense $S_0 \rightarrow S_2$ bands at 326–368 nm that should be attributed to $\pi \rightarrow \pi^*$ type transitions of carbonyl groups [7b], and weak broad bands centered at about 458 nm which are attributed to $n \rightarrow \pi^*$ type transitions, and even extend to the visible region. These similar absorption spectra are owing to their similar molecular structures. Compared to **1** that shows intense bands at 335 nm, compound **2** with electron-withdrawing substituent on the phenyl ring shows the blue-shifted absorption band (326 nm), conversely, compounds **3**, **5**, **6** and **7** with electron-donating substituents on the phenyl ring exhibit the red-shifted absorption bands in the range of 353 nm and 368 nm. Interestingly, compound **4** with strong electron-donating substituent ($-N(CH_3)_2$) on the phenyl ring even leads to all absorption bands (440, 478 and 503 nm) in the visible region. The blue-shifted absorption band of compound **2** may be ascribed to its lower HOMO energy level owing to the electron-withdrawing effect of nitro group, while the red-shifted absorption bands of compounds **3**, **5**, **6** and **7** can be attributed to higher HOMO energy level owing to the electron-donating effect of donating electron groups. It is obvious that compared to **3**, **5** and **6**, compound **7** with weak electron-donating triazolyl group leads to fewer red-shift, however, **4** with strong electron-donating *N*,*N*′-dimethylamine group, that effectively elevates HOMO energy level of phenyl ring, occurs obvious red-shift (Fig. 4).

3.3. Phosphorescence of compounds **1**–**7** in the solution

Fig. 5 shows the photoluminescence (PL) spectra of compounds **1**–**7** in the dilute (10 μM) DMF solution at room temperature, after omitting the contributions from the DMF solvent. The signals of

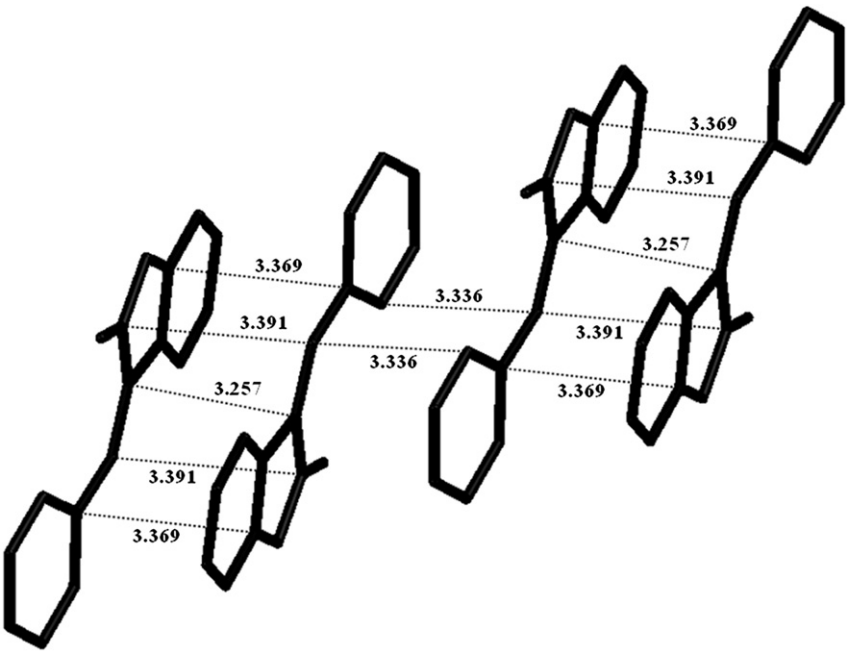

Fig. 3. The columnar stacking chain in **1**.

shorter than 500 nm may be attributed to contributions from the DMF solvent (Fig. S3, in the Supporting Information). Indeed, in the dilute (10 μM) DMSO solution (Fig. S4, in the Supporting Information), these compounds exhibit similar PL spectra to in DMF solution. The PL spectra of compounds **1**–**7** in the DMF solution are similar; they all exhibit broad emission peaks centered at about 546–578 nm, upon excitation at 365 nm. The similar emission peaks are relative to their similar molecular structures, however, the slight differences of maximal emission peaks among all seven compounds should be ascribed to electronic and steric effect of different substituents on the phenyl ring. Surprisingly, the decay lifetime of compounds **1**–**7** in the dilute solution was determined to be $\tau = 16.8–18.5$ μs (Fig. 6), upon excitation at 365 nm, indicative of the phosphorescent nature which might be assigned to the carbonyl effects in molecules, because carbonyl group can exhibit somewhat spin–orbit coupling at the carbonyl oxygen that allows for intrinsic triplet generation through intersystem crossing [7b,11].

3.4. Phosphorescence of compounds *1*–*4* in the solid state

Because many highly emissive dyes can become weak luminescent or even nonemissive in the solid state, to examine whether **1**–**7** were phosphorescent in the solid state, we investigated their PL spectra decay behaviors. As shown in Fig. 7, the decay lifetime of **1**–**7** in the solid state was determined to be $\tau = 29.0$, 26.6, 26.5, 24.3, 22.9, 23.7 and 23.7 μs, respectively. The microsecond-order decay lifetimes confirm their phosphorescent nature in the solid state at room temperature. Different from solution state, **1**–**7** exhibit longer decay lifetimes in the solid state, probably attributable to stacking effects.

In the solution, upon excitation at 365 nm, compounds **1**–**4** exhibit similar PL spectra (Fig. 5) and emit similar yellow light as indicated by the CIE chromaticity diagrams (Fig. S5, in the Supporting Information). In the solid state, the room-temperature PL spectra of **1** and **3** display maximal emission peaks at about 570 nm

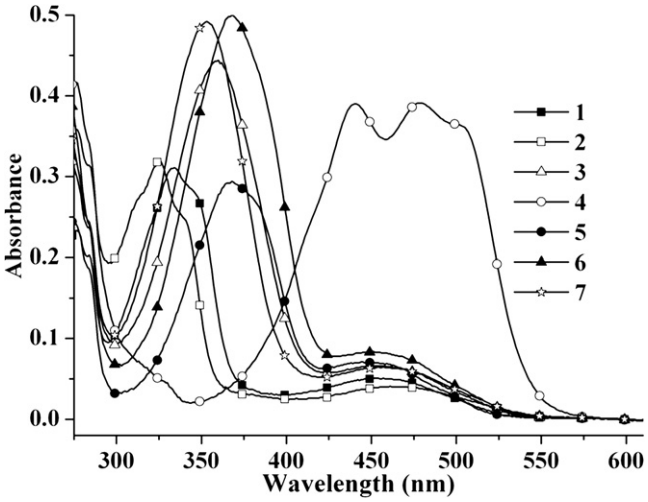

Fig. 4. UV/vis absorption spectra of **1**–**7** in 10 μM DMF solution at 298 K.

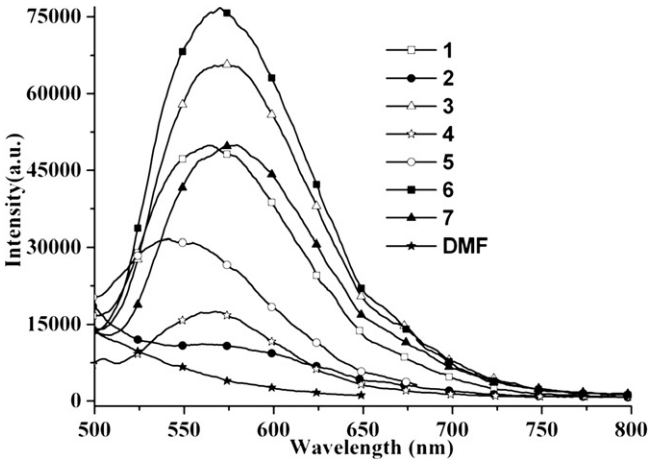

Fig. 5. PL spectra of compounds **1**–**7** (>500 nm) in the dilute DMF solution.

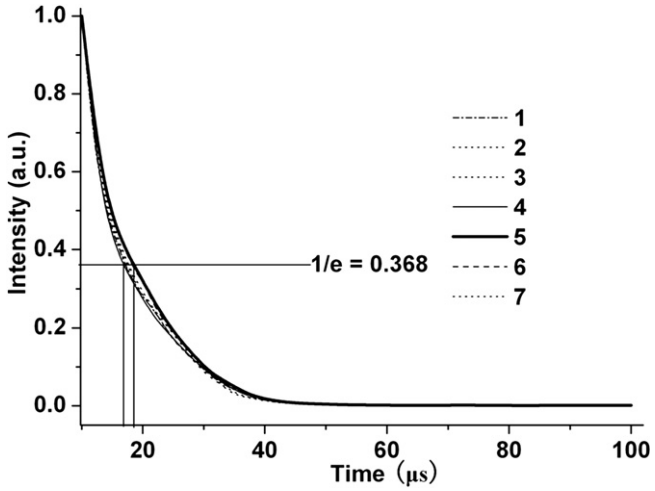

Fig. 6. The decay lifetime curves of compounds **1**–**7** in the dilute DMF solution at room temperature. The lifetime (τ) is defined as the time in which the emission intensity decays to $1/e$ of the initial intensity (I_o), where e is the natural log constant and is equal to 2.718. ($I = I_o e^{-(t/\tau)} \geq \tau = t \geq I = (1/e)I_o$) [15].

(Fig. 8), upon excitation at 365 nm, implying they emit yellow solid phosphorescence, as indicated by their CIE chromaticity diagrams (Fig. S6, in the Supporting Information). However, the room-temperature solid PL spectra of **2** and **4** exhibit maximal emission peaks at 598 and 615 nm, respectively (Fig. 8), upon excitation at 365 nm, indicating that **2** and **4** emit orange and red solid phosphorescence, respectively, as indicated by the CIE chromaticity diagrams (Fig. S6, in the Supporting Information).

It should be noted that **2** and **4** reveal stacking-induced phosphorescent color changes in the solid state, regardless of their similar phosphorescent colors in the solution. The red and bright orange red phosphorescence for **2** and **4** can even be seen with the naked eye when solid is illuminated with a 365-nm UV light at room temperature (Figs. S7 and S8, in the Supporting Information). Indeed, the yellow solid phosphorescence for **1** and **3** can also be seen with the naked eye when solid is illuminated with a 365-nm UV light at room temperature (Figs. S7 and S8, in the Supporting Information). Interestingly, the bright orange red phosphorescence for **4** even can be observed under laboratory lighting condition, indicating that the bright orange red phosphorescence of **4** can be excited in the visible region, such as 560 nm excitation light (Fig. 9).

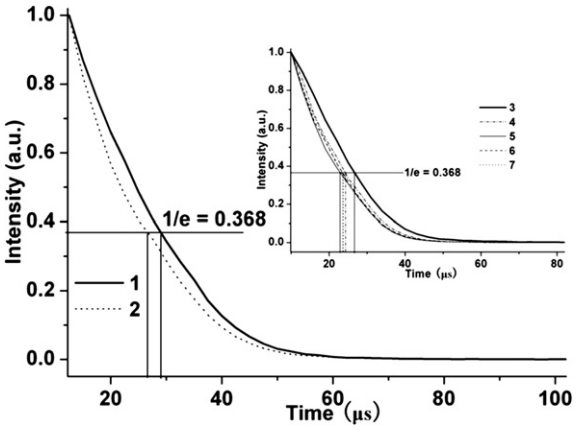

Fig. 7. The decay lifetime curves of **1**, **2** and **3**–**7** (inset) in the solid state at room temperature.

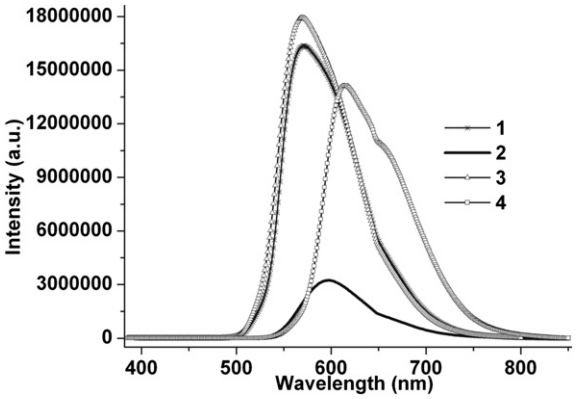

Fig. 8. Room-temperature solid PL spectra of **1**–**4** upon excitation at 365 nm.

3.5. *Phosphorescence of compounds **5**, **6** and **7** in the solid state*

The room-temperature solid PL spectra of compounds **5**, **6** and **7** are shown in Fig. 10, which display maximal emission peaks at about 589, 579 and 596 nm, respectively, upon excitation at 365 nm. Regardless of their similar PL spectra (Fig. 5), and similar yellow phosphorescence (excitation at 365 nm) as indicated by their CIE chromaticity diagrams (Fig. S9, in the Supporting Information) in the solution, in the solid state, **5** and **7** exhibit similar aurantiacus phosphorescence (excitation at 365 nm) as indicated by the CIE chromaticity diagrams (Fig. S10, in the Supporting Information), which can also be attributed to the stacking-induced phosphorescent color changes, but, **6** still emits yellow phosphorescence (Figs. S10 and S11, in the Supporting Information). Interestingly, the solid phosphorescent colors (orange) for **5** and **7** taken under ambient condition and 365-nm UV light illumination are almost consistent, indicating that the phosphorescence can be excited in the visible region, such as 550 nm excitation light (Fig. 9).

Seven phosphorescent dyes based on (*E*)-3-benzylideneimidazo [1,2-*a*] pyridin-2(3*H*)-one derivatives display similar photophysical properties (Figs. 4 and 5), and similar yellow phosphorescence (excitation at 365 nm) in the solution at room temperature. The slight differences in the photophysical properties among all seven compounds should be ascribed to electronic and steric effect of different substituents on the phenyl ring. To the best of our knowledge, the purely organic dyes that are visible phosphorescent in the solution at room temperature has not been reported.

It is noticeable that compounds **2**, **4**, **5** and **7** exhibit the stacking-induced phosphorescent color changes (from yellow phosphorescence in the solution to aurantiacus–red phosphorescence in the

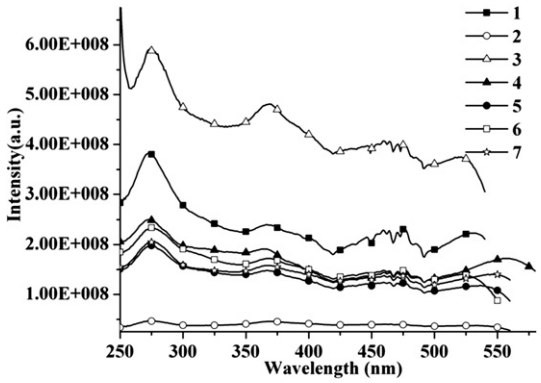

Fig. 9. Solid excitation spectra of compounds **1**–**7** at room temperature.

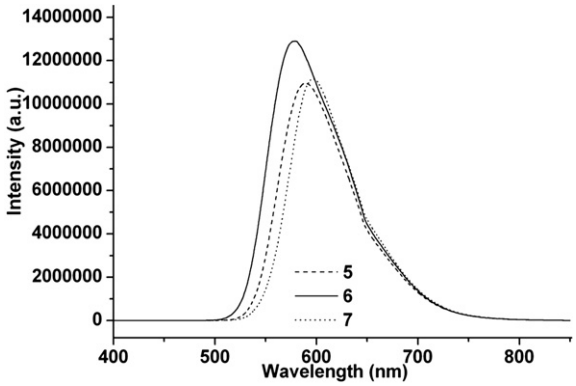

Fig. 10. Room-temperature solid PL spectra of **5**, **6** and **7** upon excitation at 365 nm.

solid state, upon excitation at 365 nm) at room temperature. Because **2**, **4**, **5** and **7** contain the hydrogen bonding acceptor group ($-NO_2$, $-N(CH_3)_2$, and N atom in imidazole and triazole ring, respectively), these hydrogen bonding acceptor groups can probably increase lateral intermolecular hydrogen bonding interactions between neighboring columns (similar to Fig. S1, in the Supporting Information), which are helpful to charge transfer between columns, further leading to lower energy emissions, as a result, these compounds emit aurantiacus to red phosphorescence in the solid state. Interestingly, these four dyes show similar phosphorescent colors taken under ambient condition and 365 nm UV light illumination, indicating that the phosphorescence can even be excited in the visible region, such as about 555 nm excitation light (Fig. 9). The similar solid-state phosphorescent colors for **2**, **4**, **5** and **7** in the visible light and ultraviolet light (365 nm) are very interesting in purely organic phosphorescent dyes. On the other hand, compounds **1**, **3** and **6** do not display the stacking-induced phosphorescent color changes, which still emit the yellow phosphorescence (excitation at 365 nm) in the solid state at room temperature, similar to that in the solution. However, under ambient condition, they show aurantiacus to orange phosphorescence. More strikingly, seven phosphorescent dyes possess longer solid-state decay lifetimes than that in the solution (Figs. 6 and 7), implying that stacking not only induces phosphorescent enhancement effect, but leads to longer decay lifetime as well. The stacking-induced phosphorescent enhancement can be demonstrated by obvious difference in quantum yields between solution state and solid state: in the DMF solution, the quantum yield of **1**–**7** is 0.016, 0.016, 0.017, 0.0021, 0.0018, 0.017 and 0.018%, respectively; in the solid state, the quantum yield of **1**–**7** is 1.3, 1.2, 1.7, 1.0, 1.1, 1.5 and 1.2%, respectively.

It should be noted that such a new class of purely organic phosphorescent dyes are promising candidates for potential applications including organic electronics such as organic light-emitting diodes for display or ambient lighting [16]. Benefits for purely organic materials (compared to organometallics) may exist in terms of costs and tunable phosphorescent colors (achieve yellow phosphorescence and low-energy red phosphorescence).

4. Conclusion

In conclusion, in this work, for the first time, we discovered a novel class of purely organic phosphorescent dyes in the solution at room temperature. This opens up the broad class of purely organic compounds to new applications in phosphor design. A carbonyl group has been found to be key structural feature to activate phosphorescent emission from pure organic dyes in the solution. The ordered columnar stacking arrangements, intermolecular close contacts, and lateral intermolecular hydrogen bonding interactions between neighboring columns make these luminogenic molecules highly phosphorescent in the solid state at room temperature, and lead to phosphorescent color changes (from yellow phosphorescence in the solution to aurantiacus to red phosphorescence in the solid state). Interestingly, some dyes show phosphorescent colors taken under ambient conditions closely resemble those measured at 365 nm UV light illumination, indicating that the phosphorescence of these compounds can even be excited in the visible region. The phosphorescence nature of these compounds is further supported by the long decay lifetimes.

Acknowledgments

We appreciate the financial support from the National Nature Science Foundation of China (21172210 and 20872135).

Appendix A. Supplementary material

CCDC 853989 contains the supplementary crystallographic data for **1**. The data can be obtained free of charge from The Cambridge Crystallographic Data Centre via www.ccdc.cam.ac.uk/data_request/cif. Supplementary data associated with this article can be found, in the online version, at doi:10.1016/j.dyepig.2012.04.003.

References

[1] (a) Birks JB. Photophysics of aromatic molecules. London, UK: Wiley; 1970;
(b) Malkin J. Photophysical and photochemical properties of aromatic compounds. Boca Raton, FL: CRC; 1992.
[2] (a) Jakubiak R, Bao Z, Rothberg R. Dendritic side groups as three-dimensional barriers to aggregation quenching of conjugated polymer fluorescence. Synth Met 2000;114:61–4;
(b) Chen L, Xu S, McBranch D, Whitten D. Tuning the properties of conjugated polyelectrolytes through surfactant complexation. J Am Chem Soc 2000;122:9302–3;
(c) Hecht S, Frechet JMJ. Dendritic encapsulation of function: applying nature's site isolation principle from biomimetics to materials science. Angew Chem Int Ed 2001;40:74–91;
(d) Setayesh S, Grimsdale AC, Weil T, Enkelmann V, Müllen K, Meghdadi F, et al. Polyfluorenes with polyphenylene dendron side chains: toward non-aggregating, light-emitting polymers. J Am Chem Soc 2001;123:946–53;
(e) Gaylord BS, Wang S, Heeger AJ, Bazan GC. Water-soluble conjugated oligomers: effect of chain length and aggregation on photoluminescence-quenching efficiencies. J Am Chem Soc 2001;123:6417–8.
[3] (a) Luo JD, Xie ZL, Lam JWY, Cheng L, Chen HY, Qiu CF, et al. Aggregation-induced emission of 1-methyl-1,2,3,4,5-pentaphenylsilole. Chem Commun; 2001:1740–1;
(b) An BK, Kwon SK, Jung SD, Park SY. Enhanced emission and its switching in fluorescent organic nanoparticles. J Am Chem Soc 2002;124:14410–5;
(c) Chen J, Law CCW, Lam LWY, Dong YQ, Lo SMF, Williams ID, et al. Synthesis, light emission, nanoaggregation, and restricted intramolecular rotation of 1,1-substituted 2,3,4,5-tetraphenylsiloles. Chem Mater 2003;15:1535–46;
(d) Li Z, Dong YQ, Lam JWY, Sun JX, Qin AJ, Haëussler M, et al. Functionalized siloles: versatile synthesis, aggregation-induced emission, and sensory and device applications. Adv Funct Mater 2009;19:905–17;
(e) Hong YN, Lam JWY, Tang BZ. Aggregation-induced emission: phenomenon, mechanism and applications. Chem Commun; 2009:4332–53.
[4] Baldo MA, Thompson ME, Forrest SR. Phosphorescent materials for application to organic light emitting devices. Pure Appl Chem 1999;71:2095–106.
[5] Kohler A, Wilson JS, Friend RH. Fluorescence and phosphorescence in organic materials. Adv Mater 2002;14:701–7.
[6] (a) De Silva AP, Gunaratne HQN, Gunnlaugsson T, Huxley AJM, McCoy CP, Rademacher JT, et al. Signaling recognition events with fluorescent sensors and switches. Chem Rev 1997;97:1515–66;
(b) Baldo MA, O'Brien DF, You Y, Shoustikov A, Sibley S, Thompson ME, et al. Highly efficient phosphorescent emission from organic electroluminescent devices. Nature 1998;395:151–4;
(c) Rumsey WL, Vanderkooi JM, Wilson DF. Imaging of phosphorescence: a novel method for measuring oxygen distribution in perfused tissue. Science 1988;241:1649–51;
(d) Shao Y, Yang Y. Efficient organic heterojunction photovoltaic cells based on triplet materials. Adv Mater 2005;17:2841–4;
(e) Zhang G, Palmer GM, Dewhirts MW, Fraser CL. A dual-emissive-materials design concept enables tumour hypoxia imaging. Nat Mater 2009;8:747–51.

[7] (a) Yuan WZ, Shen XY, Zhao H, Lam JWY, Tang L, Lu P, et al. Crystallization-induced phosphorescence of pure organic luminogens at room temperature. J Phys Chem C 2010;114:6090–9;
(b) Bolton O, Lee K, Kim HJ, Lin KY, Kim J. Activating efficient phosphorescence from purely organic materials by crystal design. Nat Chem 2011;3:205–10.
[8] (a) Yong GP, Li CF, Li YZ, Luo SW. New zwitterionic radical salts: dimers in solution and unusual magnetic and luminescent properties in the solid state. Chem Commun 2010;46:3194–6;
(b) Li YZ, Yong GP, Zhang YM, Li CF, She WL. 3-Carbaldehyde-substituted 2,3′-biimidazo[1,2-*a*]pyridin-2′-one radicals: Interesting π-stacking structures and magnetic properties. Synth Met 2011;161:713–7;
(c) Zhang YM, Yong GP, Li CF, She WL, Li YZ. The zwitterionic radical and its neutral radical derivative with interesting magnetic properties. Synth Met 2012;161:2708–13.
[9] (a) Yong GP, Qiao S, Wang ZY. A one-dimensional coordination polymer based on novel radical anion ligand generated in situ: notable magnetic and luminescence properties. Cryst Growth Des 2008;8:1465–7;
(b) Yong GP, Li YZ, Li CF, Zhang YM, She WL. New metal–anion radical framework materials: Co^{II} compounds showing ferromagnetic to antiferromagnetic phase transition at about 344 K, and Zn^{II} compounds exhibiting terminal anion ligand induced direct white-light-emission. Dalton Trans 2011;40:4131–9;
(c) Yong GP, Li YZ, She WL, Zhang YM. Isostructural metal–anion radical coordination polymers with tunable phosphorescent colors (deep blue, blue, yellow, and white) induced by terminal anions and metal cations. Chem Eur J 2011;17:12495–501;
(d) Yong GP, Li YZ, Zhang YM, She WL. Magnetic and luminescent properties of Cd(II)- and Fe(II)-anion radical frameworks: various networks or structures influenced by metal ion sizes or in situ forming mechanisms of anion radical ligand. Cryst Eng Comm 2012;14:1439–48.
[10] Yong GP, Zhang YM, She WL, Li YZ. Stacking-induced white-light and blue-light phosphorescence from purely organic radical materials. J Mater Chem 2011;21:18520–2.
[11] (a) Kearns DR, Case WA. Investigation of singlet→triplet transitions by the phosphorescence excitation method. III. Aromatic ketones and aldehydes. J Am Chem Soc 1966;88:5087–97;
(b) Itoh T. The evidence showing that the intersystem crossing yield of benzaldehyde vapour is unity. Chem Phys Lett 1988;151:166–8.
[12] (a) Reindel F, Von Putzer-Reybegg A. Über die umsetzungs-produkte von pyrimidazolon-2 mit aromatischen aldehyden und ringförmigen 1,2-dicarbonylverbindungen. Ber Dtsch Chem Ges 1926;59:2926–32;
(b) Abramovitch RA, Hey DH. The condensation of 2,3-dihydro-2-oxoimidazo [1,2-*a*]pyridine with o-nitrobenzaldehyde. J Chem Soc C; 1966:1095–6.
[13] Li CF, Yong GP, Li YZ. Phosphorescent iridium (III) 2-phenylpyridine complexes: efficient color tuning by novel ancillary ligands. Inorg Chem Commun 2010;13:179–82.
[14] Sheldrick GM. SHELXL-97 and SHELXS-97. Göttingen, Germany: University of Göttingen; 1998.
[15] Stylianou KC, Heck R, Chong SY, Bacsa J, Jones JTA, Khimyak YZ, et al. A guest-responsive fluorescent 3D microporous metal–organic framework derived from a long-lifetime pyrene core. J Am Chem Soc 2010;132:4119–30.
[16] Kim SH, Park S, Kwon JE, Park SY. Organic light-emitting diodes with a white-emitting molecule: emission mechanism and device characteristics. Adv Funct Mater 2011;21:644–51.